

Conformational Control of Energy Transfer: A Mechanism for Biocompatible Nanocrystal-Based Sensors**

Euan R. Kay, Jungmin Lee, Daniel G. Nocera, and Mounqi G. Bawendi*

Recent advances have given access to a myriad of engineered nanomaterials, ranging from functional nanotubes and fluorescent nanocrystals (NCs) to oligonucleotide self-assemblies and polymer nanoparticles. The integration of these nanomaterials with dynamic molecular components will likely be a key component in realizing their full potential.^[1] In this regard, combining NCs with molecular machines presents an unexplored strategy for modulating NC properties in response to a specific stimulus. Herein, we outline this new approach by designing a self-referencing, NC/nanomachine-based sensor. A conformational switch, activated by a chosen specific analyte (here, H⁺ ions), is used to vary the efficiency of energy transfer between the NC and an appended species. The analyte concentration is reported by a ratiometric fluorescence signal that is quantifiable and robust across a variety of imaging conditions, allowing for the high-resolution measurement of pH within individual endosomes in HeLa cells. This study thus exemplifies the strategy of disconnecting sensing and reporting functions to create a universal fluorescent sensor design that addresses many of the challenges associated with harnessing the unique optical properties of NCs.

Several intrinsic properties serve to make NC fluorophores useful for advanced imaging applications,^[2] such as intravital multi-photon laser scanning microscopy, multiplexing, and single-receptor tracking.^[3] In particular, their narrow and tunable emission spectra, high quantum yields, broad absorption profiles, high photostability, and large single and multi-photon cross sections have made NCs useful complements to organic fluorophores and fluorescent proteins. These

attributes provide strong motivation for finding ways to incorporate NCs into fluorescent sensors. Fluorescent sensors with the optical properties of NCs will enable the non-invasive quantification of biochemical species with high spatial and temporal resolution and with the ability to track changes over extended periods of time within complex living environments.^[4]

One of the most promising concepts for constructing NC sensors is to attach a second chromophore (such as an organic dye or a transition-metal complex) that can act as a fluorescence resonant energy transfer (FRET) partner with the NC.^[5] NC fluorophores make ideal FRET donors—their narrow emission features can easily be tuned to match the absorption spectrum of any acceptor, thus endowing the sensing construct with the favorable optical properties of the NC. However, existing NC-based fluorescent sensors have yet to demonstrate good performance. While analyte-induced cleavage,^[6] displacement,^[7] or chemical modification^[8] can irreversibly modulate a FRET interaction and confer detection abilities on an NC construct, continuous monitoring of analyte levels requires a reversible response to analyte concentration. Furthermore, fluorescent sensing within living environments must ultimately address confounding factors such as variations in probe concentration, excitation intensity, and collection efficiency,^[8a,9] necessitating a self-referencing output, commonly achieved by taking a ratio of fluorescence intensities at two different wavelengths. The majority of reported NC-based sensors have thus exploited analyte-sensitive dyes to provide both sensing and signaling functions, but resulting in several significant shortcomings, including the limited variety of available analyte-responsive dyes and difficulty of use in biological environments.^[10,6a]


Herein, we introduce a different approach that circumvents these limitations by separating the optical signaling from the chemical sensing components. A chemically insensitive NC-molecule FRET pair is connected through a linker that undergoes a reversible conformational change upon binding to the analyte (Figure 1 a). As energy-transfer interactions are extremely sensitive to distance, conformational changes in the linker lead to a substantial change in optical signal. Monitoring the emission from both fluorophores therefore provides a sensitive, ratiometric response that can be used to track analyte concentrations within microscopic biological environments. Maintaining specific pH values and gradients is essential for many biological processes such as protein folding. Furthermore, in the extracellular space, low pH is an important indicator of many tumor microenvironments. These bio-applications and others provide an imperative for improved fluorescent sensors that are capable of

[*] Dr. E. R. Kay,^[5] J. Lee,^[4] Prof. D. G. Nocera, Prof. M. G. Bawendi
Department of Chemistry,
Massachusetts Institute of Technology
77 Massachusetts Ave., Cambridge, MA 02139-4307 (USA)
E-mail: mgb@mit.edu
Homepage: <http://nanocluster.mit.edu>

[†] Current address: EaStChem School of Chemistry
University of St. Andrews
North Haugh, St. Andrews, KY16 9ST (UK)

[‡] These authors contributed equally to this work.

[**] E.R.K. was supported by The Royal Commission for the Exhibition of 1851. The work received support from the NIH through grants 5-U54-CA151884-03 (M.G.B.) and 5R01CA126642-02 (M.G.B., D.G.N). The Biophysical Instrumentation Facility for the Study of Complex Macromolecular Systems and DCIF at MIT (NSF-0070319, NIH GM68762 and CHE-980806, DBI-979582) are gratefully acknowledged.

 Supporting information for this article (experimental details) is available on the WWW under <http://dx.doi.org/10.1002/anie.201207181>.

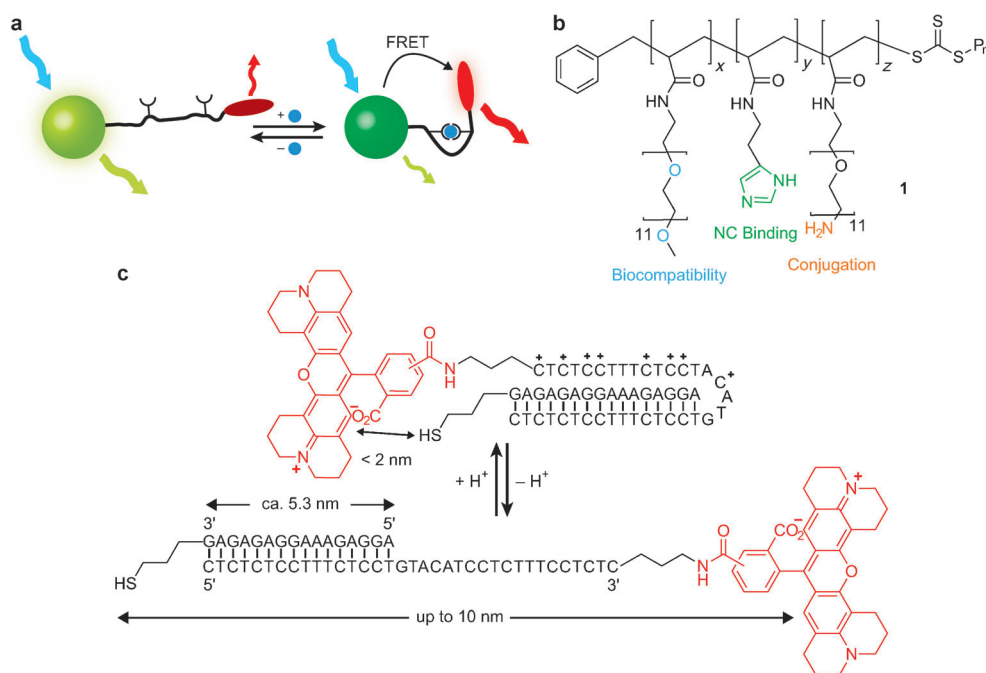


Figure 1. Sensor design and constituent parts. a) Schematic illustration of sensor design wherein a fluorescent NC (green) is conjugated to one or several molecular fluorophores (red) through an analyte-sensitive linker. Binding of a specific analyte (blue) to the linker triggers a conformational change that alters the donor-acceptor distance and changes the FRET efficiency. b) Chemical formula of PIL ligand **1**. Monomer units are arranged randomly; ratio $x:y:z$ is 1:2:1, and typically $x+y+z \approx 16$ (i.e., an average of 32 monomer units per chain). c) pH-Responsive oligonucleotide triplex/duplex conformational switch, bearing carboxy-X-rhodamine (red) and thiol functionalities. Not drawn to scale.

accurately monitoring pH values in living systems with high spatial and temporal resolution.^[11]

Certain cytosine-rich oligonucleotide sequences are known to undergo folding or unfolding in response to changes in pH, depending on the protonation state of the cytosine imino group.^[12] Recently, a ratiometric pH sensor was created by appending two molecular fluorophores to one such sequence, allowing pH changes in the endosomes of haemocytes to be monitored.^[13] To create an NC-based sensor in which a reversible conformational change is transduced into an optical response, a simpler pH-responsive oligonucleotide was selected (Figure 1c). This sequence is capable of cycling between two well-defined conformations: an extended duplex-overhang structure and a folded CT-motif triplex. The effective pK_a for this transition is ideal for achieving greatest sensitivity in mildly acidic biological environments.^[14] The relatively rigid DNA adduct helps to ensure that the two ends of the switch are held far apart in the unfolded state. Protonation of cytosine imino groups in the single-stranded region results in folding to allow Hoogsteen triplet base-pairing interactions in the major groove of the duplex. This conformational change dramatically alters the distance between the termini of the DNA adduct (Figure 1c). To build the NC-based pH sensor, 5(6)-carboxy-X-rhodamine (Rox)—a pH-insensitive fluorophore—was conjugated to the 3' overhanging end of the 35-mer (Figure 1c). At the opposite end of the construct, a thiol at the 3' terminus of the 16-mer acted as a point of attachment for polymer-coated NCs.

We have previously demonstrated compact, biocompatible, and bright NCs based on polymeric imidazole ligands (PILs) such as **1** (Figure 1b).^[15] Water-soluble CdSe/CdS core-shell NCs, emitting at 560 nm, were prepared using PIL **1**. Activation of the primary amines with the heterobifunctional linker sulfosuccinimidyl-4-(*N*-maleimidomethyl)cyclohexane-1-carboxylate (sulfo-SMCC) allowed covalent attachment to the thiol on the hybridized double-stranded oligonucleotide (see Supporting Information for details). Successful conjugation of the oligonucleotide to the nanoparticles was confirmed by the UV/Vis absorption spectrum, featuring both the inorganic NC and organic dye peaks (Supporting Information, Figure S2). A linear fit of this spectrum to a reference NC and DNA-Rox

spectra gave an average coupling stoichiometry of 3.6 DNA-Rox units per NC.

When placed in phosphate buffers of varying pH and excited at 460 nm, the construct exhibits emission that does not vary with time and is comprised of two features at wavelengths corresponding to the NC ($\lambda_{PL,max} = 560$ nm) and Rox ($\lambda_{PL,max} = 610$ nm) components (Figure 2a). Because Rox absorbs minimally at 460 nm, this indicates excitation through energy transfer from the NC. Upon varying the pH values from 8.0 to 6.1, a dramatic change in the relative intensity of these two features is observed (Figure 2). At high pH values, strong emission from the NC and poor FRET efficiency to Rox is observed, which is consistent with the unfolded oligonucleotide switch holding the donor and acceptor fluorophores far apart. As the pH value is lowered, NC emission becomes increasingly quenched, with concomitant enhancement of emission from the Rox. This is consistent with increasing FRET efficiency from the NC to Rox as the folded triplex conformation of the oligonucleotide brings the NC energy donor and Rox energy acceptor closer in space.

A practical parameter for expressing sensor response is the proportion of green channel emission (using 590 nm as a cutoff) compared to the total integrated emission. A plot of this ratio shows a sigmoidal response (Figure 2b, black squares), with maximum sensitivity around pH 7.0, in line with the characteristics of the oligonucleotide conformational switch.^[14] This pH range for conformational switching is ideal for imaging mildly acidified biological microenvironments. The sensor response was found to be unaffected by changes in

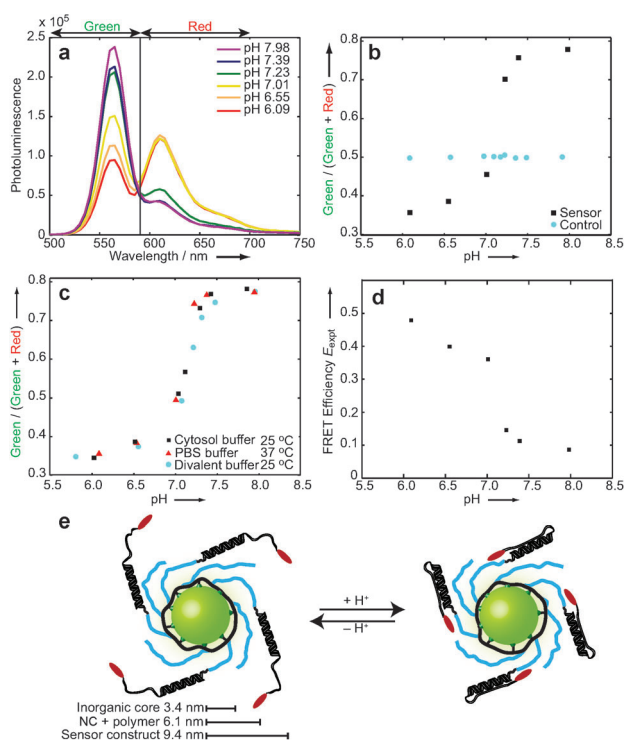


Figure 2. Spectroscopic characterization of the sensor. a) Sensor photoluminescence spectra on excitation at 460 nm in PBS buffers with differing pH values at 25 °C. Solid black line at 590 nm indicates cutoff wavelength for integration of intensities in the “green” and “red” channels. Spectra were corrected for variation in concentration using absorbance measurement at excitation wavelength. b) Proportion of total emission intensity in the “green” channel (as defined in (a)) as pH is varied at 25 °C for the sensor (black squares) and a control NC-Rox construct that lacks the oligonucleotide switch. c) Sensor performance under varying environmental conditions. PBS (phosphate buffered saline): 10 mM phosphate, 137 mM Na⁺, 2.7 mM K⁺; Cytosol buffer: 10 mM phosphate, 139 mM K⁺, 12 mM Na⁺; Divalent buffer: 12 mM phosphate, 137 mM NaCl, 2.7 mM KCl, 0.9 mM Ca²⁺, 0.5 mM Mg²⁺. d) Efficiency of energy transfer from NC to Rox components with varying pH. e) Cartoon representation of the sensor construct and operation, indicating the inorganic core radius as determined by TEM and hydrodynamic radii of unfunctionalized and functionalized water-soluble NC constructs, as determined by DLS (see Supporting Information for further details).

both temperature and in electrolyte content (Figure 2c), it was reproducible across several samples, and the construct could be recovered, stored, and re-used with no adverse effects (see Supporting Information). Furthermore, a control construct with Rox dyes coupled directly to amino-PIL-coated NCs with no oligonucleotide linker showed no variation in the ratio of emission across the same pH range (Figure 2b, blue circles).

A deeper understanding of the underlying chemomechanical and photophysical processes can be gained by examining the Förster model, which describes well the efficiency of energy transfer from an NC to an acceptor conjugated to it. When multiple acceptors are conjugated to each NC, the ensemble FRET response can be reproduced by assuming a Poisson distribution of coupling stoichiometries.^[16] The equations for these calculations are presented in the Support-

ing Information. Comparing a set of modeled FRET efficiencies to the experimentally observed efficiencies (Figure 2d) at low and high pH, we can infer that the donor–acceptor separations in the all-folded and all-unfolded states are 6.3 nm and 9.4 nm, respectively (Figure S11). These values are consistent with the physical dimensions of the sensor construct found by dynamic light-scattering (DLS) measurements (Figure 2e). The hydrodynamic radius of the sensor was found to be invariant with pH at 9.4 nm. This corresponds very well with the donor–acceptor distance calculated for the unfolded state using FRET theory and suggests that the size of the nanoconstruct is defined by the double-stranded DNA region (including its solvation shell) irrespective of pH. In the unfolded state, the single-stranded component does not extend into solution beyond the existing solvation shell. Furthermore, the hydrodynamic radius of the PIL-coated NCs prior to conjugation with the DNA was measured as 6.1 nm, suggesting that in the folded state the Rox dye is located as close to the NC as possible (6.3 nm from FRET), without penetrating the polymer coating.

Robust maintenance of the sensor response under a variety of environmental conditions *in vitro* gives us confidence that the design can be applied to image pH variation in living systems. As a proof of concept, we probed the pH of endosomes in human adenocarcinoma cells. It is well known that during endosome maturation, there is a significant pH drop from early endosomes to the late endosomes through the action of H⁺-ATPases,^[17] yet it remains challenging to probe live cell endosome pH values, track the acidification of endosomes over time, and develop a complete understanding of this dynamic process.

The response of our sensor was first calibrated by imaging it in buffers of varying pH under a confocal microscope. The sample was excited at 488 nm and the image acquired simultaneously in the green NC channel (560–580 nm) and the red Rox channel (590–620 nm). The proportion of green channel intensity as a fraction of the total intensity at different pH values is shown in Figure 3a. Although absolute intensities are affected by changing excitation wavelength and green and red channel widths, the power of the ratiometric approach is that the sigmoidal sensor response is maintained (Figure 3a, black squares). The control construct, which lacks the oligonucleotide conformational switch, again shows no such variation in photoluminescence (PL) response with pH.

HeLa cells were then incubated with the sensor constructs at 37 °C for ten minutes, allowing uptake by endocytosis. Following rinsing to remove excess sensor, the incubation at 37 °C was continued for 0, 10, 20, and 30 minutes prior to imaging. Qualitatively, punctate staining characteristic of endosomes was apparent in all healthy cells examined, with these features closer to the center of each cell at later time points. As illustrated in Figure 3b, the images were processed to calculate the average proportion of green channel fluorescence (see Supporting Information for details) for each identifiable endosomal structure within multiple cells at each time point. The ratio values (Figure 3c) show a clear decrease with increasing time, consistent with progressive acidification of the endosomes. No such variation was observed upon incubation of cells with the control construct, which lacks the

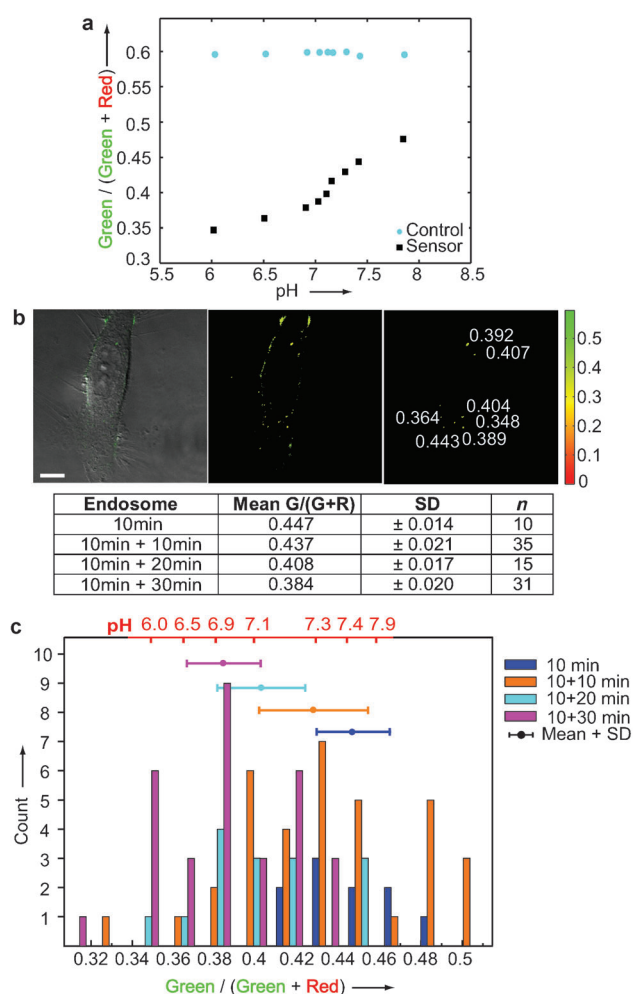


Figure 3. Application of the sensor for confocal imaging of endosomal pH in live cells. a) Proportion of total emission in the green channel upon confocal imaging of the sensor (black squares) and the control (blue circles) constructs in phosphate buffers with varying pH. b) Representative raw image, false-colored ratiomap, and endosomes picked from a cell from the 10 min + 20 min group. Scale bar = 10 μ m. c) Emission ratios for endosomes found in cells incubated with the sensor construct for a 10 min pulse period followed by 0, 10 min, 20 min, and 30 min chase periods (endosomes $n=10, 35, 15, 31$, respectively).

oligonucleotide conformational switch (Figure S10). Comparing the ratio values with those from the calibration (Figure 3a) reveals an average drop in pH value from greater than 7.4 to less than 6.9 over the course of the experiment, with significant numbers of vesicles showing pH values of approximately 6.0 by the last time point recorded.

Our pH resolution here is limited by the variation in the number of DNA-Rox moieties per NC. The Poisson distribution of stoichiometries that describes the construct population gives rise to a distribution of fluorescence ratios. At the single NC level, individual sensors will exhibit different emission profiles for the same pH, depending on the number of appended DNA-Rox units. This effect becomes significant for endosomes whose sizes can only accommodate on the order of a dozen NC sensors, giving rise to a distribution of measured pH values at any given time point. Although the

natural biological variability in pH amongst endosomes has been found to be as high as ± 0.2 pH units,^[18] the variability in construct stoichiometry can be assigned as the major contributor to the distribution in observed pH values within the same time points of this experiment (error bars, Figure 3c). This distribution is also reflected in the range of ratios obtained using the non-sensing control constructs (error bars, Figure S7).

The application of NCs to study complex living systems has the potential to yield molecular level information with unprecedented spatial resolution, together with the ability to track changes over long periods of time. Using molecular machines to control the optical properties of NC constructs presents a new and flexible approach to designing sensors. By transducing a mechanical property rather than an optical property, we separate the sensing and signaling functions. Such sensors are no longer constrained to operate within the parameters defined by the available analyte-sensitive fluorophores. The conjugation strategies employed herein are universal and so any FRET pair of fluorophores can be used; this includes the possibility of creating all-NC ratiometric sensors. Likewise, the conformational switch may be optimized to the analyte and concentration range without needing to change the fluorescent components or imaging setup. Oligonucleotide conformational switches triggered by other simple stimuli have been characterized,^[12] along with DNA-based aptamers that exhibit a conformational change upon binding non-nucleotide targets,^[19] and supramolecular chemistry has provided a host of synthetic receptors that undergo a conformational change upon guest binding.^[20] The sensor design reported herein demonstrates that any of these systems may be harnessed in an NC-nanomachine sensor. Achieving control over nanoconstruct stoichiometry is a key challenge that now must be addressed. Although applications that involve imaging large numbers of NC fluorophores (such as mapping the tumor environment) are not limited by the distribution of NC valencies, NC constructs with precisely defined stoichiometry would also allow quantitative measurement for applications involving only a few NC sensors.

Received: September 4, 2012

Published online: December 6, 2012

Keywords: biosensors · fluorescent probes · molecular devices · molecular machines · quantum dots

[1] R. Klajn, J. F. Stoddart, B. A. Grzybowski, *Chem. Soc. Rev.* **2010**, 39, 2203–2237.

[2] a) M. Bruchez, Jr., M. Moronne, P. Gin, S. Weiss, A. P. Alivisatos, *Science* **1998**, 281, 2013–2016; b) W. C. W. Chan, S. M. Nie, *Science* **1998**, 281, 2016–2018.

[3] a) D. R. Larson, W. R. Zipfel, R. M. Williams, S. W. Clark, M. P. Bruchez, F. W. Wise, W. W. Webb, *Science* **2003**, 300, 1434–1436; b) M. Stroh, J. P. Zimmer, D. G. Duda, T. S. Levchenko, K. S. Cohen, E. B. Brown, D. T. Scadden, V. P. Torchilin, M. G. Bawendi, D. Fukumura, R. K. Jain, *Nat. Med.* **2005**, 11, 678–682; c) O. T. Bruns, H. Itrich, K. Peldschus, M. G. Kaul, U. I. Tromsdorf, J. Lauterwasser, M. S. Nikolic, B. Mollwitz, M. Merkel, N. C. Bigall, S. Sapra, R. Reimer, H. Hohenberg, H.

- Weller, A. Eychmüller, G. Adam, U. Beisiegel, J. Heeren, *Nat. Nanotechnol.* **2009**, *4*, 193–201.
- [4] I. L. Medintz, H. T. Uyeda, E. R. Goldman, H. Mattoussi, *Nat. Mater.* **2005**, *4*, 435–446.
- [5] R. C. Somers, M. G. Bawendi, D. G. Nocera, *Chem. Soc. Rev.* **2007**, *36*, 579–591.
- [6] a) M. Suzuki, Y. Husimi, H. Komatsu, K. Suzuki, K. T. Douglas, *J. Am. Chem. Soc.* **2008**, *130*, 5720–5725; b) K. Boeneman, B. C. Mei, A. M. Dennis, G. Bao, J. R. Deschamps, H. Mattoussi, I. L. Medintz, *J. Am. Chem. Soc.* **2009**, *131*, 3828–3829.
- [7] a) I. L. Medintz, A. R. Clapp, H. Mattoussi, E. R. Goldman, B. Fisher, J. M. Mauro, *Nat. Mater.* **2003**, *2*, 630–638; b) R. Freeman, T. FINDER, L. Bahshi, I. Willner, *Nano Lett.* **2009**, *9*, 2073–2076.
- [8] a) R. Freeman, R. Gill, I. Shweky, M. Kotler, U. Banin, I. Willner, *Angew. Chem.* **2009**, *121*, 315–319; *Angew. Chem. Int. Ed.* **2009**, *48*, 309–313; b) S. Wang, M.-Y. Han, D. Huang, *J. Am. Chem. Soc.* **2009**, *131*, 11692–11694.
- [9] I. L. Medintz, M. H. Stewart, S. A. Trammell, K. Susumu, J. B. Delehanty, B. C. Mei, J. S. Melinger, J. B. Blanco-Canosa, P. E. Dawson, H. Mattoussi, *Nat. Mater.* **2010**, *9*, 676–684.
- [10] a) P. T. Snee, R. C. Somers, G. Nair, J. P. Zimmer, M. G. Bawendi, D. G. Nocera, *J. Am. Chem. Soc.* **2006**, *128*, 13320–13321; b) J. M. Dubach, D. I. Harjes, H. A. Clark, *J. Am. Chem. Soc.* **2007**, *129*, 8418–8419; c) Y. Chen, R. Thakar, P. T. Snee, *J. Am. Chem. Soc.* **2008**, *130*, 3744–3745; d) E. J. McLaurin, A. B. Greytak, M. G. Bawendi, D. G. Nocera, *J. Am. Chem. Soc.* **2009**, *131*, 12994–13001; e) T. Jin, A. Sasaki, M. Kinjo, J. Miyazaki, *Chem. Commun.* **2010**, *46*, 2408–2410; f) J. D. Krooswyk, C. M. Tyrakowski, P. T. Snee, *J. Phys. Chem. C* **2010**, *114*, 21348–21352; g) X. Wang, C. Boschetti, M. J. Ruedas-Rama, A. Tunnacliffe, E. A. H. Hall, *Analyst* **2010**, *135*, 1585–1591; h) L. E. Page, X. Zhang, A. M. Jawaid, P. T. Snee, *Chem. Commun.* **2011**, *47*, 7773–7775; i) R. C. Somers, R. M. Lanning, P. T. Snee, A. B. Greytak, R. K. Jain, M. G. Bawendi, D. G. Nocera, *Chem. Sci.* **2012**, *3*, 2980–2985.
- [11] a) L. Albertazzi, B. Storti, L. Marchetti, F. Beltram, *J. Am. Chem. Soc.* **2010**, *132*, 18158–18167; b) M. Tantama, Y. P. Hung, G. Yellen, *J. Am. Chem. Soc.* **2011**, *133*, 10034–10037.
- [12] J. Bath, A. J. Turberfield, *Nat. Nanotechnol.* **2007**, *2*, 275–284.
- [13] S. Modi, M. G. Swetha, D. Goswami, G. D. Gupta, S. Mayor, Y. Krishnan, *Nat. Nanotechnol.* **2009**, *4*, 325–330.
- [14] M. Brucale, G. Zuccheri, B. Samorì, *Org. Biomol. Chem.* **2005**, *3*, 575–577.
- [15] W. H. Liu, A. B. Greytak, J. Lee, J. Park, C. R. Wong, L. F. Marshall, W. Jiang, P. N. Curtin, A. Y. Ting, D. G. Nocera, R. K. Jain, M. G. Bawendi, *J. Am. Chem. Soc.* **2010**, *132*, 472–483.
- [16] T. Pons, I. L. Medintz, X. Wang, D. S. English, H. Mattoussi, *J. Am. Chem. Soc.* **2006**, *128*, 15324–15331.
- [17] I. Mellman, R. Fuchs, A. Helenius, *Annu. Rev. Biochem.* **1986**, *55*, 663–700.
- [18] M. Serresi, R. Bizzarri, F. Cardarelli, F. Beltram, *Anal. Bioanal. Chem.* **2009**, *393*, 1123–1133.
- [19] J. W. Liu, Z. H. Cao, Y. Lu, *Chem. Rev.* **2009**, *109*, 1948–1998.
- [20] L. Kovbasyuk, R. Krämer, *Chem. Rev.* **2004**, *104*, 3161–3187.